

Synergy between c-di-GMP and quorum-sensing signaling in *Vibrio cholerae* biofilm morphogenesis

Jojo A. Prentice¹, Andrew A. Bridges¹, Bonnie L. Bassler^{1,2#}

#Correspondence to: bbassler@princeton.edu

Affiliations:

¹Department of Molecular Biology, Princeton University, Princeton, New Jersey 08544, USA.

²The Howard Hughes Medical Institute, Chevy Chase, MD 20815, USA.

Key words:

Biofilm morphogenesis | *Vibrio cholerae* | quorum sensing | c-di-GMP| signal transduction

Abstract

1 Transitions between individual and communal lifestyles allow bacteria to adapt to changing
2 environments. Bacteria must integrate information encoded in multiple sensory cues to
3 appropriately undertake these transitions. Here, we investigate how two prevalent sensory inputs
4 converge on biofilm morphogenesis: quorum sensing, which endows bacteria with the ability to
5 communicate and coordinate group behaviors, and second messenger c-di-GMP signaling, which
6 allows bacteria to detect and respond to environmental stimuli. We use *Vibrio cholerae* as our
7 model system, the autoinducer AI-2 to modulate quorum sensing, and the polyamine
8 norspermidine to modulate NspS-MbaA-mediated c-di-GMP production. Individually, AI-2 and
9 norspermidine drive opposing biofilm phenotypes, with AI-2 repressing and norspermidine
10 inducing biofilm formation. Surprisingly, however, when AI-2 and norspermidine are
11 simultaneously detected, they act synergistically to increase biofilm biomass and biofilm cell
12 density. We show that this effect is caused by quorum-sensing-mediated activation of *nspS-mbaA*
13 expression, which increases the levels of NspS and MbaA, and in turn, c-di-GMP biosynthesis, in
14 response to norspermidine. Increased MbaA-synthesized c-di-GMP activates the VpsR

15 transcription factor, driving elevated expression of genes encoding key biofilm matrix
16 components. Thus, in the context of biofilm morphogenesis in *V. cholerae*, quorum-sensing
17 regulation of c-di-GMP-metabolizing receptor levels connects changes in cell population density
18 to detection of environmental stimuli.

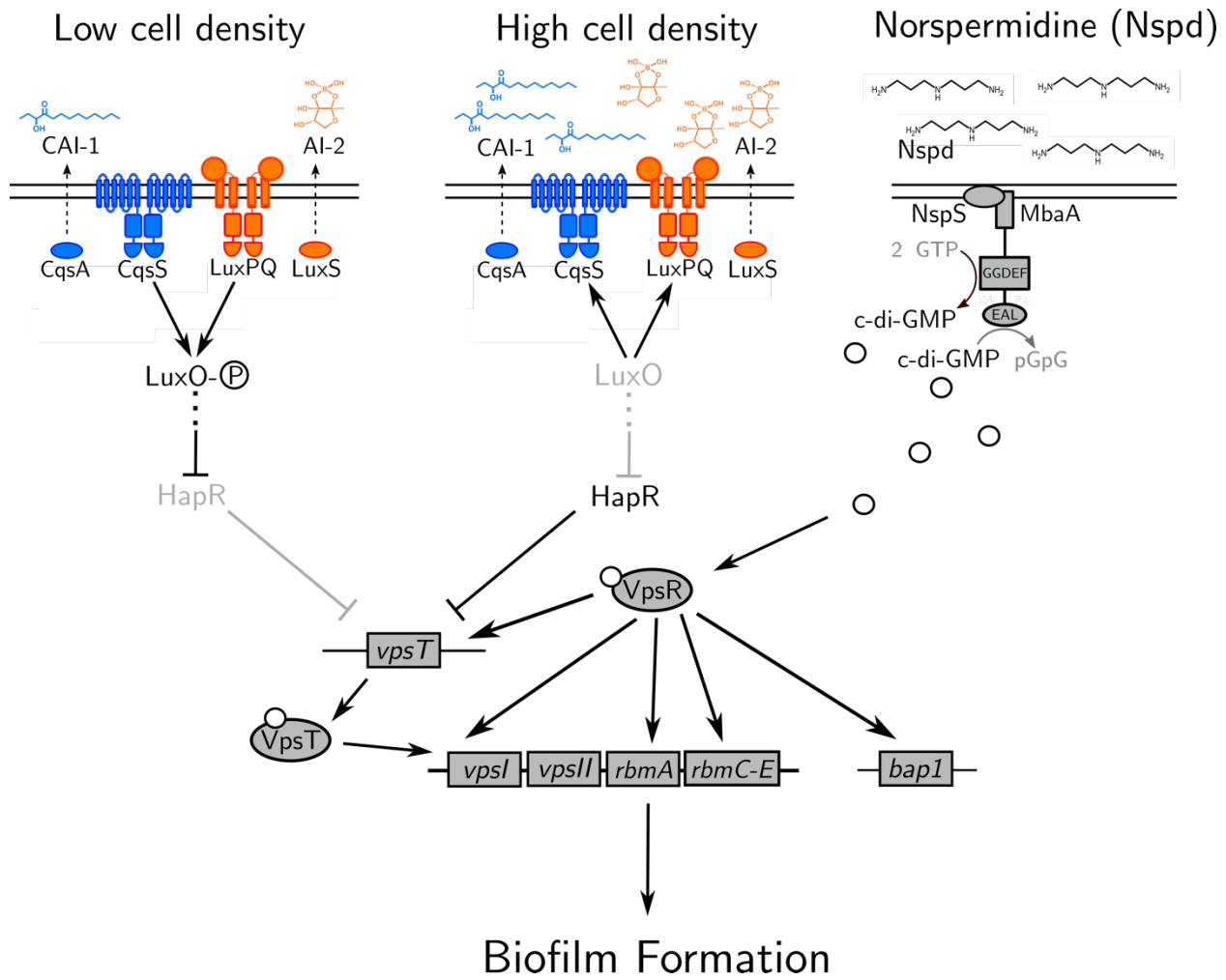
Importance

19 The development of multicellular communities, known as biofilms, facilitates beneficial functions
20 of gut microbiome bacteria and makes bacterial pathogens recalcitrant to treatment.
21 Understanding how bacteria regulate the biofilm lifecycle is fundamental to biofilm control in
22 industrial processes and in medicine. Here, we demonstrate how two major sensory inputs –
23 quorum-sensing communication and second messenger c-di-GMP signaling – jointly regulate
24 biofilm morphogenesis in the global pathogen *Vibrio cholerae*. We characterize the mechanism
25 underlying a surprising synergy between quorum-sensing and c-di-GMP signaling in controlling
26 biofilm development. Thus, the work connects changes in cell population density to detection of
27 environmental stimuli in a pathogen of clinical significance.

Introduction

28 Bacteria often integrate multiple sensory cues into the control of behaviors including the
29 formation of biofilms – surface-associated bacterial communities encapsulated in self-produced
30 extracellular matrices (1). The biofilm lifestyle confers advantages to constituent members,
31 including protection against antibiotics, predation, and shear stress (2–4). Indeed, biofilms are a
32 predominant form of bacterial life in the environment, in industrial processes, and in disease (5).

33 In the global pathogen and model biofilm-forming bacterium *Vibrio cholerae*, two well-
34 studied sensory inputs control the biofilm lifecycle. The first is quorum sensing: a cell-cell
35 communication process that orchestrates collective behaviors (6). Quorum sensing relies on the
36 production, release, and group-wide detection of extracellular signaling molecules called
37 autoinducers (7). *V. cholerae* possesses five quorum-sensing autoinducer-receptor pairs, two of
38 which are key to the present work, diagrammed in Fig. 1 (8). At low cell density, the autoinducer
39 receptors CqsS and LuxPQ are unliganded and function as kinases, channeling phosphate to the
40 response regulator LuxO (9,10). LuxO~P indirectly represses the gene encoding the high cell
41 density master regulator HapR (11,12). HapR represses expression of the vibrio polysaccharide
42 biosynthetic genes (*vpsI* and *vpsII* operons), *vpsT*, encoding a transcriptional activator of the *vpsI*
43 and *vpsII* operons, and *rbmA* and *rbmC-E*, encoding biofilm matrix proteins. Thus, in the low cell
44 density quorum-sensing regime, when *hapR* is repressed, VPS and biofilm matrix protein levels
45 are high, and *V. cholerae* forms biofilms (13). At high cell density, cholerae autoinducer-1 (CAI-
46 1) and autoinducer-2 (AI-2) accumulate and bind CqsS and LuxPQ respectively, converting them
47 from kinases to phosphatases. Phosphate is stripped from LuxO, which inactivates it (9,10). As a
48 result, HapR is produced, it suppresses biofilm formation, and biofilm dispersal occurs (Fig. 1)
49 (12).



50 Fig. 1. Model showing the contributions of quorum-sensing and norspermidine signaling
 51 to biofilm gene expression. See text for details. The P in the circle represents phosphate.
 52 White circles represent c-di-GMP. Norspermidine, Nspd.

53 The second major regulator of the *V. cholerae* biofilm lifecycle is the second messenger
 54 molecule cyclic diguanylate (c-di-GMP). c-di-GMP is produced and degraded by enzymes
 55 containing diguanylate cyclase and/or phosphodiesterase activities, respectively. These activities
 56 are commonly modulated by environmental stimuli including light, temperature, amino acids,
 57 oxygen, and polyamines (14–18). High intracellular c-di-GMP levels drive biofilm formation via
 58 binding to and activation of the VpsT and VpsR transcription factors. VpsT-c-di-GMP and VpsR-

59 c-di-GMP both activate expression of the *vpsI* and *vpsII* operons, and additionally, VpsR-c-di-
60 GMP activates expression of *rbmA*, *rbmC-E*, and *bap1*. By contrast, when cytoplasmic c-di-GMP
61 levels are low, biofilm formation is repressed, favoring the motile state (Fig. 1) (18,19). Thus, in
62 *V. cholerae*, the low cell density quorum-sensing regime and high levels of cytoplasmic c-di-GMP
63 each promote biofilm formation, whereas the high cell density quorum-sensing regime and low
64 levels of cytoplasmic c-di-GMP each repress biofilm formation. Attempts to knit together the *V.*
65 *cholerae* quorum-sensing and c-di-GMP pathways have revealed two key findings: first, high
66 cytoplasmic c-di-GMP concentrations can override negative quorum-sensing regulation of biofilm
67 genes (21,22). Second, the high cell density quorum-sensing regime activates the expression of
68 genes encoding over a dozen diguanylate cyclases and phosphodiesterases, while repressing
69 only a few genes encoding such enzymes (8,21).

70 Here, we investigate the integration of quorum-sensing and c-di-GMP information in *V.*
71 *cholerae* biofilm morphogenesis, from ligand detection to population-scale biofilm changes. We
72 use exogenous administration of the AI-2 autoinducer to modulate quorum-sensing activity and
73 we use administration of the polyamine norspermidine to control the activity of the NspS-MbaA c-
74 di-GMP-metabolizing circuit (Fig. 1) (17). We find that as expected, quorum sensing represses
75 biofilm formation in the absence of NspS-MbaA detection of norspermidine. However,
76 surprisingly, quorum sensing increases biofilm biomass and biofilm cell density when MbaA-
77 mediated c-di-GMP synthesis is stimulated by norspermidine supplementation. We show that this
78 positive quorum-sensing effect occurs because at high cell density, HapR activates *nspS-mbaA*
79 expression, which drives increased NspS and MbaA production and consequently, increased c-
80 di-GMP production when the norspermidine ligand is present. The increased c-di-GMP activates
81 VpsR, which in turn, activates *rbmA* matrix gene expression, resulting in the formation of larger
82 and denser biofilms. We propose a model in which quorum sensing represses biofilms, but also
83 primes the bacterial population to optimally respond to environmental stimuli that foster c-di-GMP
84 production. Our findings reveal a new mechanism by which *V. cholerae* modulates its biofilm

85 lifecycle and, moreover, they show that quorum sensing does not strictly repress *V. cholerae*
86 biofilm formation.

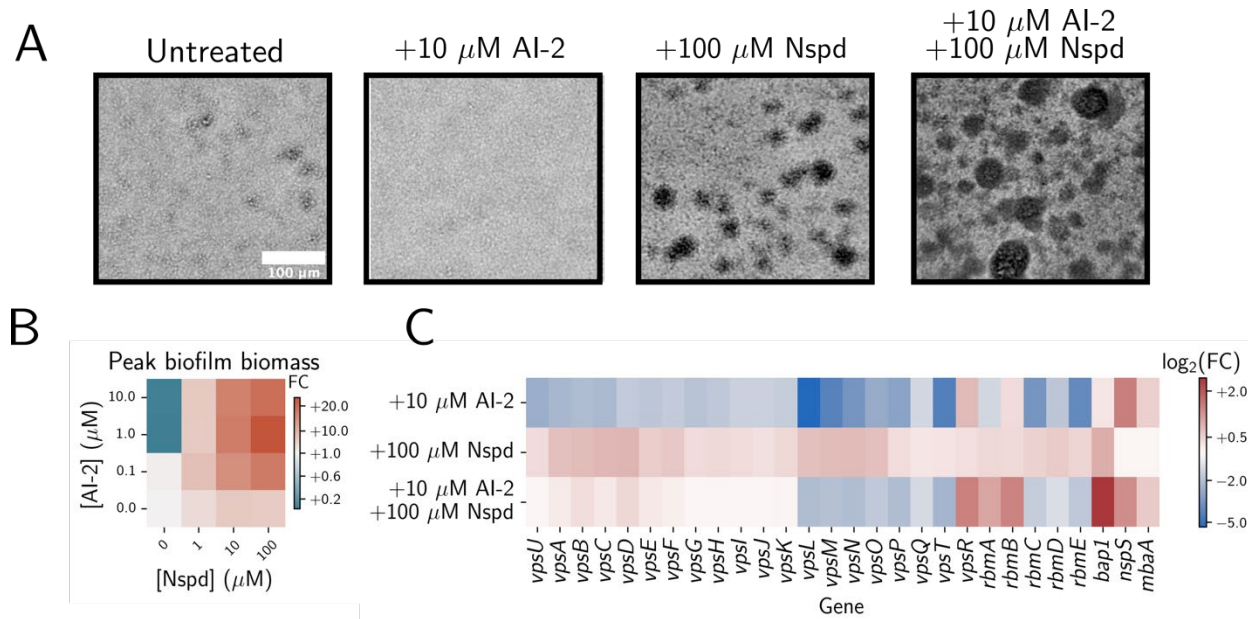
Results

Quorum sensing elevates norspermidine-driven increases in biofilm biomass in *V. cholerae*

87 To investigate how *V. cholerae* integrates information from c-di-GMP and quorum-sensing
88 signaling into the control of the biofilm lifecycle, we measured biofilm phenotypes across quorum-
89 sensing and c-di-GMP signaling regimes. To simplify the regulation of quorum sensing, we used
90 a *V. cholerae* strain harboring only a single quorum-sensing receptor that controls LuxO
91 phosphorylation – the AI-2 receptor LuxPQ. Moreover, we deleted the AI-2 synthase *luxS* so that
92 quorum sensing is exclusively controlled through exogenous administration of AI-2. We refer to
93 this strain as the “AI-2-responsive strain.” First, we measured biofilm biomass accumulation over
94 time in the AI-2-responsive strain in the absence of AI-2 (i.e., in the low cell density quorum-
95 sensing regime, Fig. 2A,B). Consistent with previous findings, in this signaling regime, biofilms
96 formed (Fig. 2A) (13). Addition of saturating AI-2 (i.e., to achieve the high cell density quorum-
97 sensing regime, Fig. 2A,B) prevented the AI-2-responsive strain from forming biofilms, again,
98 consistent with previous findings (13,21,23). To investigate how changes in c-di-GMP affect
99 biofilm formation in the low and high cell density quorum-sensing regimes, we provided
100 exogenous norspermidine to drive c-di-GMP production. Norspermidine had only a modest effect
101 on peak biofilm biomass when the AI-2-responsive *V. cholerae* strain was in the low cell density
102 quorum-sensing regime, whereas, surprisingly, norspermidine drove dramatically increased
103 biofilm biomass when the strain was in the high cell density quorum-sensing regime (Fig. 2A,B).
104 These results were independent of the specific autoinducer-receptor pair used to stimulate
105 quorum sensing in *V. cholerae*, as we likewise modulated quorum sensing in a CAI-1-responsive
106 strain and obtained analogous results (Fig. S1A).

107 To assess whether the combination of the CAI-1 and AI-2 cues altered the balance
 108 between quorum-sensing repression of biofilm gene expression and quorum-sensing synergy
 109 with norspermidine, we supplemented a strain that is responsive to both CAI-1 and AI-2 (i.e., that
 110 lacks both *cqsA* and *luxS*) with norspermidine, the CqsS agonist, and AI-2 and measured the
 111 effects on biofilm biomass. The triple combination resulted in roughly equivalent biofilm biomass
 112 accumulation as did supplementation with norspermidine and AI-2 in the AI-2-responsive strain
 113 (Fig. S1B). Thus, we conclude that the synergy between quorum-sensing and norspermidine
 114 signaling is a general feature of the high cell density quorum-sensing regime.

115 Crucially, biofilm biomass did not increase in the high cell density quorum-sensing and
 116 high norspermidine regime when *mbaA* was deleted (Fig. S1C). This result shows that changes
 117 in biofilm biomass are mediated by the known polyamine-sensing NspS-MbaA pathway. Thus,
 118 although quorum sensing and norspermidine independently drive opposing biofilm phenotypes,
 119 with quorum-sensing repressing and c-di-GMP promoting biofilm formation, together, they
 120 function synergistically to increase biofilm biomass in *V. cholerae*.



123 responsive strain after 14 h growth with the indicated treatments. (B) Quantitation of peak biofilm
124 biomass for the AI-2-responsive strain grown with the indicated treatments, displayed as a
125 heatmap. Data are normalized as fold changes relative to the untreated AI-2-responsive strain
126 (bottom left corner). (C) Heatmap of \log_2 fold changes in biofilm gene expression in the AI-2-
127 responsive strain grown with the indicated treatments normalized to that of the untreated strain.
128 Samples were collected at $OD_{600} = 0.1$. Norspermidine, Nspd; Fold change, FC.

129 To define the gene expression changes underlying the quorum-sensing and
130 norspermidine signaling synergy in *V. cholerae* biofilm morphogenesis, we conducted RNAseq in
131 the AI-2-responsive strain under each condition shown in Fig. 2A. Treatment with AI-2 alone drove
132 a reduction in *vps* operon, *vpsT*, *rbmA*, and *rbmC-E* expression, consistent with previous findings
133 and with repression of biofilm formation (Fig. 2C) (21,24). Conversely, treatment with
134 norspermidine caused a modest elevation in *vps* operon and *bap1* expression (Fig. 2C).
135 Simultaneous treatment with AI-2 and norspermidine reduced *vps* operon, *vpsT*, and *rbmC-E*
136 expression and increased *vpsR*, *rbmA*, and *bap1* expression. These results suggest that quorum
137 sensing and norspermidine act synergistically to elevate biofilm biomass through a mechanism
138 that decouples *vps* polysaccharide biosynthesis gene expression from expression of genes
139 encoding the matrix proteins RbmA and Bap1.

HapR activates *nspS-mbaA* expression at high cell density, which increases both c-di-GMP production and biofilm biomass in response to norspermidine

140 To explore the unexpected result that quorum sensing enhances norspermidine-driven
141 increases in biofilm biomass in *V. cholerae*, we began by measuring effects on c-di-GMP – the
142 immediate output of the MbaA circuit in response to norspermidine. To do this, we employed a
143 fluorescent, riboswitch-based reporter of c-di-GMP levels (25,26). Surprisingly, although provision
144 of AI-2 alone repressed biofilm formation (Fig. 2A,B), c-di-GMP reporter output was modestly
145 elevated in the high cell density quorum-sensing state (Fig. 3A). We considered possible roles for

146 quorum-sensing master regulators in modulating c-di-GMP levels. It is known that the HapR high
147 cell density master transcription factor drives c-di-GMP degradation eliminating it as a candidate
148 (Fig. 1) (26). Thus, we suspected that the low cell density quorum-sensing master regulators –
149 the Qrr1-4 small RNAs and/or the AphA transcription factor – could reduce c-di-GMP levels at low
150 cell density. If so, repression of the low cell density master regulators at high cell density could
151 underpin the increase in c-di-GMP that occurs following AI-2 treatment. Deletion of *aphA* in a low
152 cell density-locked mutant strain (encoding the phosphomimic *luxO*^{D61E} allele), also lacking *hapR*
153 (*luxO*^{D61E} *ΔhapR*), increased c-di-GMP reporter output to the level of a high cell density-locked
154 mutant strain (encoding a non-phosphorylatable LuxO allele) lacking *hapR* (*luxO*^{D61A} *ΔhapR*).
155 Deletion of *qrr1-4* in the *ΔaphA ΔhapR* strain had no additional effect on c-di-GMP reporter output
156 (Fig. S2). We infer from these data that AphA, but not the Qrr sRNAs, suppresses c-di-GMP
157 reporter output in the low cell density quorum-sensing state. Thus, both the low and high cell
158 density quorum-sensing master regulators reduce c-di-GMP levels, and high cell density
159 repression of *aphA* expression explains how supplementation with AI-2 elevates c-di-GMP
160 reporter output. Notably, however, the small increase in c-di-GMP that occurs following
161 supplementation with AI-2 alone is insufficient to override HapR-mediated repression of *vpsT* and
162 the *vps* operons. Hence, biofilm formation is repressed under this treatment condition. Finally,
163 consistent with our biofilm measurements, simultaneous administration of norspermidine and AI-
164 2 drove maximal c-di-GMP reporter output (Fig. 3A).

165 Fig. 3. **HapR-mediated activation of *nspS-mbaA* expression drives quorum-sensing and**

166 **norspermidine synergy in c-di-GMP production and biofilm biomass.** (A) c-di-GMP reporter

167 output in the AI-2-responsive strain following the indicated treatments, shown as a heatmap. Data

168 are displayed as percent differences compared to the untreated strain (bottom left corner), with

169 teal representing low and purple representing high c-di-GMP reporter output, respectively. (B) c-

170 di-GMP reporter output in the Δ *hapR* AI-2-responsive strain following the indicated treatments.

171 Data are normalized as percent changes relative to the Δ *hapR* AI-2-responsive strain treated with

172 AI-2 (left bar). $N = 3$ biological replicates. (C) Top panel: western blot of MbaA-3xFLAG in the AI-

173 2-responsive strain and the Δ *hapR* AI-2-responsive strain following the indicated treatments.

174 Bottom panel: quantitation of MbaA-3xFLAG protein levels from the top panel. Data are

175 normalized as fold changes relative to the AI-2 treatment in each strain and in each replicate. N

176 = 3 biological replicates. (D) Top panel: western blot of MbaA-3xFLAG in the AI-2-responsive

177 strain (1st and 3rd lanes) and the AI-2-responsive strain carrying *Pbad-nspS-mbaA* on the
178 chromosome (2nd and 4th lanes), treated as indicated. Bottom panel: quantitation of MbaA-
179 3xFLAG protein levels from the top panel. Data in the first and second bars are normalized to
180 data in the first bar for each replicate. Data in the third and fourth bars are normalized to data in
181 the third bar for each replicate. $N = 3$ biological replicates. (E) c-di-GMP reporter output in the AI-
182 2-responsive strain carrying *Pbad-nspS-mbaA* on the chromosome. Data are normalized as
183 percent changes relative to the mean c-di-GMP output for the 0.1% arabinose treatment for each
184 group. $N = 3$ biological replicates. (F) Quantitation of peak biofilm biomass for the AI-2-responsive
185 strain and the AI-2-responsive strain carrying *Pbad-nspS-mbaA* on the chromosome, treated as
186 indicated. Images were taken at 14 h. Data are normalized as fold changes (FC) relative to the
187 AI-2-responsive strain grown with norspermidine. $N = 3$ biological replicates. In D-F, white bars
188 show results for the AI-2-responsive strain, and gray bars show results for the AI-2-responsive
189 strain carrying *pbad-nspS-mbaA-3xFLAG*. In B-F, unpaired *t*-tests were performed for statistical
190 analyses. **** $P \leq 0.0001$; *** $P \leq 0.001$; ** $P \leq 0.01$; * $P \leq 0.05$; ns $P > 0.05$. Norspermidine, Nspd;
191 Arabinose, Ara; Fold change, FC.

192 To explain how AI-2 supplementation could increase c-di-GMP levels when norspermidine
193 is present, we posited that at high cell density, HapR could activate *nspS-mbaA* expression.
194 Consequently, higher levels of NspS and MbaA would be produced, enabling increased synthesis
195 of c-di-GMP and, in turn, increased biofilm biomass in response to norspermidine. Data
196 supporting this possibility are the following: First, our RNAseq results show that in the high cell
197 density quorum-sensing regime, *nspS* and *mbaA* transcript levels are elevated (Fig. 2C). Second,
198 a mathematical model that we previously developed to capture NspS-MbaA-mediated c-di-GMP
199 production/degradation predicts that elevating NspS and MbaA concentrations should increase
200 c-di-GMP in response to norspermidine (17). Third, in the Δ *hapR* AI-2-responsive strain, c-di-
201 GMP output remained insensitive to the addition of norspermidine when AI-2 was supplied (Fig.

202 3B). Thus, a HapR-dependent mechanism must underlie the elevated sensitivity of the c-di-GMP
203 reporter to norspermidine. To test our hypothesis, we tagged MbaA with 3xFLAG and measured
204 protein levels by western blot in the AI-2-responsive strain and in the Δ hapR AI-2-responsive
205 strain in the presence and absence of AI-2. We did not measure NspS, because *nspS* and *mbaA*
206 are in an operon, and we observed that both *nspS* and *mbaA* transcript levels increased in step
207 in the high cell density quorum-sensing signaling state (Fig. 2C) (27). Indeed, MbaA levels
208 doubled following AI-2 supplementation, and moreover, this increase depended on HapR (Fig.
209 3C).

210 To probe whether increasing NspS-MbaA levels is sufficient to promote the observed
211 increase in the sensitivity of c-di-GMP biosynthesis to changes in norspermidine levels, we
212 replaced the endogenous chromosomal *nspS-mbaA* promoter with the arabinose-controlled *Pbad*
213 promoter, and additionally, we tagged MbaA with 3xFLAG. Thus, we could synthetically modulate
214 NspS-MbaA production by supplying arabinose, we could quantify MbaA levels by western blot,
215 and we could track changes in c-di-GMP production. Importantly, this strategy provided the
216 essential feature of removing quorum-sensing control of *nspS-mbaA* transcription. We identified
217 a concentration of arabinose (0.1%) that drove MbaA production to roughly the level achieved by
218 norspermidine treatment alone (Fig. 3D). We likewise identified a concentration of arabinose
219 (0.25%) that produced the doubling in MbaA production that occurs following norspermidine and
220 AI-2 co-treatment (Fig. 3D). Companion measurements of c-di-GMP reporter output showed that
221 increasing NspS and MbaA levels drove increased c-di-GMP production (Fig. 3E) for samples
222 grown with only norspermidine and with both norspermidine and AI-2. Consistent with this finding,
223 increasing NspS and MbaA levels increased biofilm biomass accumulation to roughly the same
224 extent in the presence of norspermidine alone and in the presence of both norspermidine and AI-
225 2 (Fig. 3F). Thus, we conclude that HapR-directed activation of *nspS-mbaA* expression accounts
226 for the increased sensitivity of c-di-GMP biosynthesis to norspermidine in the high cell density
227 quorum-sensing regime. Moreover, the increased sensitivity of c-di-GMP biosynthesis to

228 norspermidine results in elevated biofilm biomass in the high cell density and high norspermidine
229 signaling regime.

230 Finally, we considered the possibility that an NspS-MbaA-independent mechanism could
231 also contribute to the synergy between norspermidine and quorum-sensing signaling. For this
232 analysis, we introduced the *vpvC^{W240R}* gene encoding a constitutively active diguanylate cyclase
233 under the *Pbad* promoter onto the chromosome of the AI-2-responsive strain. This construct
234 allowed us to ramp up intracellular c-di-GMP levels via arabinose treatment. In the high cell
235 density quorum-sensing regime, no increase in biofilm biomass occurred at any level of *vpvC^{W240R}*
236 expression within the range tested, suggesting that quorum sensing does not generally enhance
237 the sensitivity of biofilm biomass to changes in c-di-GMP levels (Fig. S3). Rather, quorum sensing
238 specifically enhances norspermidine-driven increases in biofilm biomass through an NspS-MbaA-
239 directed enhancement in the sensitivity of c-di-GMP biosynthesis to norspermidine.

MbaA synthesized c-di-GMP activates VpsR

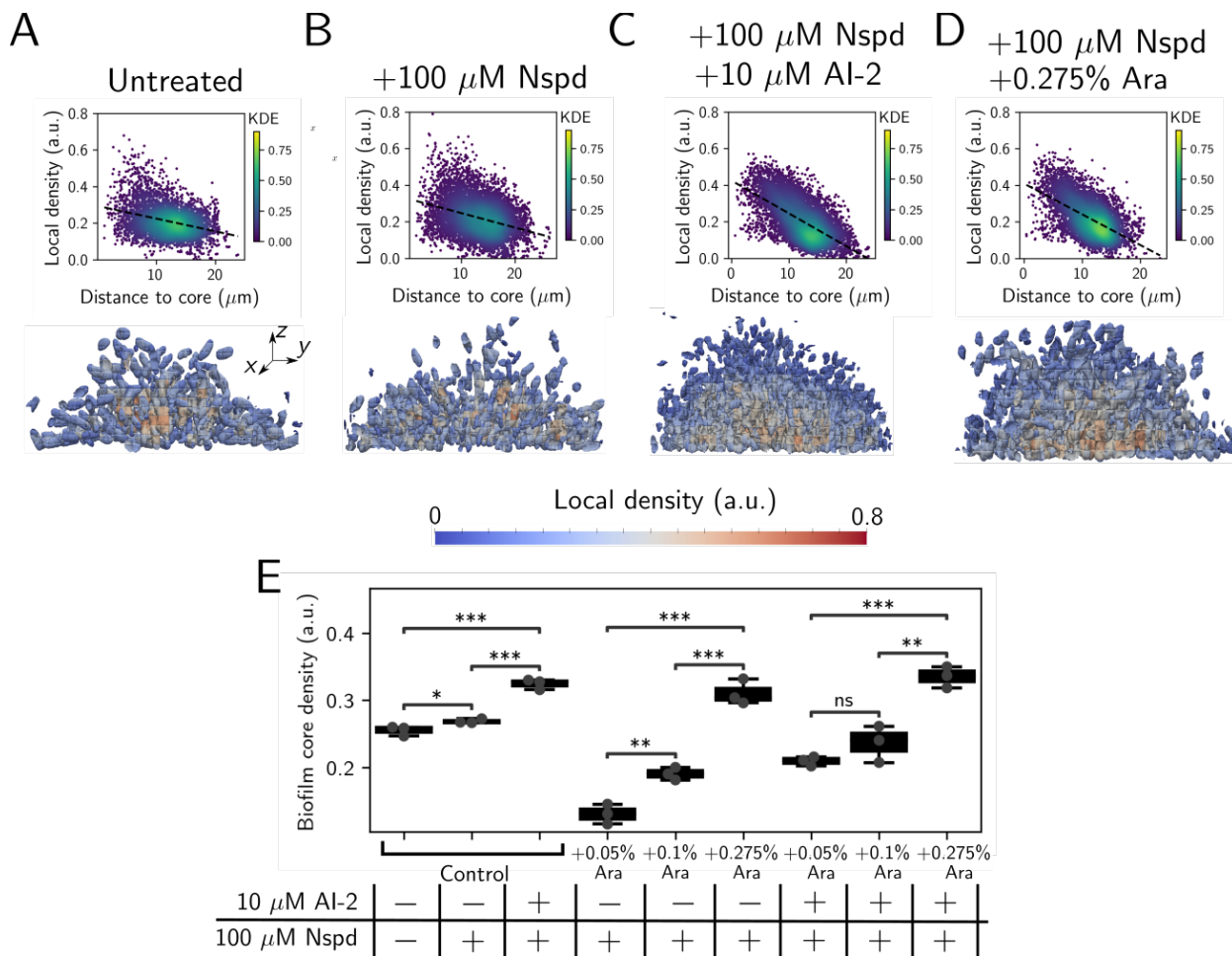
240 We sought to identify the downstream component responsible for transducing the AI-2-
241 norspermidine-driven increase in c-di-GMP into the control of biofilm biomass. We hypothesized
242 that the increased c-di-GMP produced by MbaA could activate and/or increase the levels of the
243 transcription factors VpsT and VpsR, both of which control expression of biofilm-related genes
244 (24). Consistent with our RNAseq results, VpsT-3xFLAG and VpsR-3xFLAG levels increase
245 following supplementation with both norspermidine and AI-2 compared to supplementation with
246 AI-2 alone, as does the downstream matrix protein, RbmA-3xFLAG (we note, however, that the
247 changes in VpsT-3xFLAG and VpsR-3xFLAG levels do not achieve statistical significance; Figs.
248 2C and S4). Thus, we examined the individual roles of VpsT and VpsR in controlling RbmA protein
249 levels. Regarding VpsT: in a $\Delta vpsT$ AI-2-responsive strain in the high norspermidine and high
250 quorum-sensing signaling regime, the VpsR-3xFLAG level was equivalent to that in the AI-2-
251 responsive strain following the same treatment (Fig. S4). However, the $\Delta vpsT$ AI-2-responsive

252 strain possessed lower RbmA-3xFLAG than the AI-2-responsive strain in the high norspermidine
253 and high quorum-sensing signaling regime (Fig. S4). Regarding VpsR: In the $\Delta vpsR$ AI-2-
254 responsive strain, we could not detect VpsT-3xFLAG or RbmA-3xFLAG in the high cell density
255 and high norspermidine signaling state (Fig. S4). Together, these results suggest that VpsR
256 regulates *vpsT* expression, but not vice versa, and both VpsR and VpsT independently regulate
257 *rbmA* expression. Moreover, we infer that because VpsT does not regulate *vpsR* expression, the
258 modest activation of *vpsR* expression that occurs in the high norspermidine and high quorum-
259 sensing signaling regime is a consequence of VpsR autofeedback, as shown previously (28). We
260 conclude that in the high cell density quorum-sensing and high norspermidine signaling regime,
261 HapR-mediated activation of *nspS-mbaA* increases norspermidine-driven c-di-GMP production.
262 C-di-GMP, in turn, activates VpsR. The VpsR-c-di-GMP complex activates expression of the *vps*
263 operons, *rbmA*, and, to a lesser extent, *vpsR*. VpsR-c-di-GMP also indirectly activates these same
264 genes via induction of *vpsT* expression and consequent VpsT-c-di-GMP-mediated transcriptional
265 activation.

Activation of *rbmA* expression promotes alterations in biofilm morphogenesis in the high cell density and high norspermidine signaling regime

266 To probe whether quorum-sensing and c-di-GMP signaling synergistically affect overall
267 biofilm architecture, we compared the spatial characteristics of *V. cholerae* biofilms receiving no
268 treatment, treatment with norspermidine, and treatment with both norspermidine and AI-2 using
269 single-cell resolution microscopy. We assessed the relation between cell distance from the biofilm
270 core and local cell density (i.e., how tightly-packed are the cells) for all cells in the biofilm under
271 each signaling regime. Cells in biofilms treated with both ligands resided in closer proximity to
272 one another at the biofilm core than cells in untreated biofilms or cells in biofilms treated with
273 norspermidine alone (Fig 4. A-C, E). These results indicate that the high norspermidine and high

274 cell density quorum-sensing signaling state alters global biofilm architecture, leading to
 275 densification of the biofilm core.



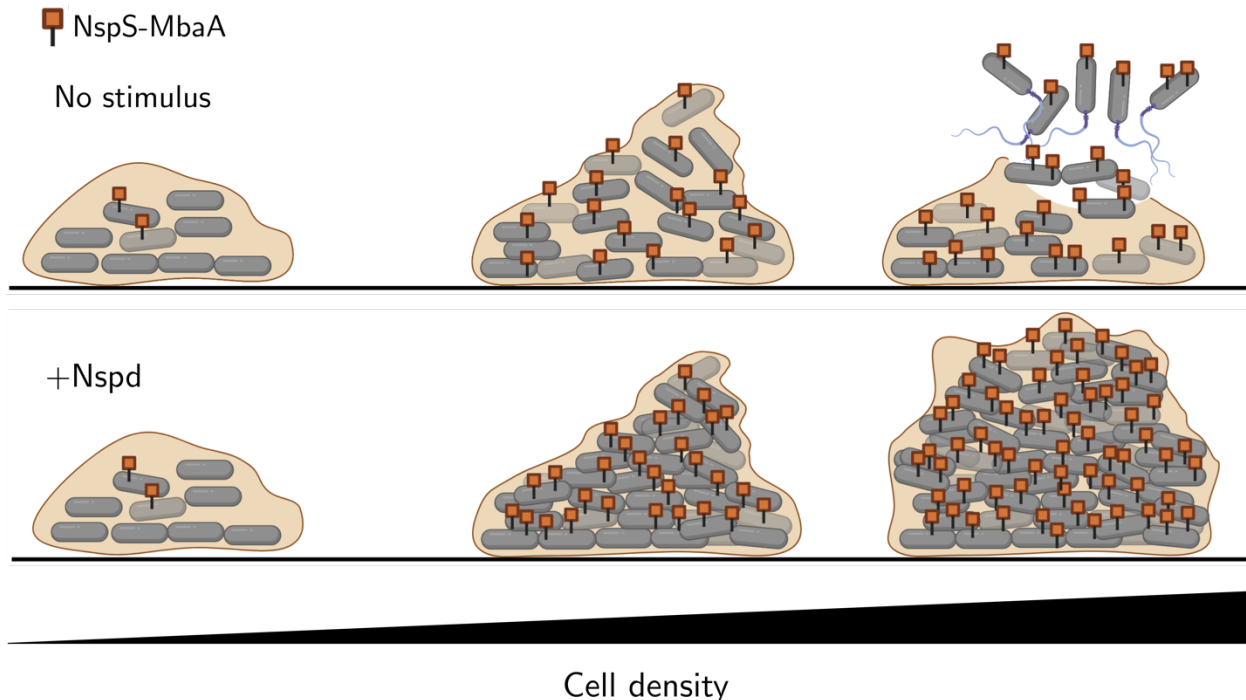
276 Fig 4. **Norspermidine and quorum-sensing signaling jointly enhance biofilm biomass**
 277 **through RbmA-mediated biofilm core densification.** (A-C) (Top panels) Scatter plots showing
 278 the relationship between local biofilm cell density and distance from the biofilm core in the AI-2-
 279 responsive strain treated as indicated. (Bottom panels) Cross-sectional 3D renderings of
 280 segmented cells in biofilms \sim 16 h post-inoculation, colored by local biofilm cell density and treated
 281 as in the top panels. (D) As in panels A-C for the $\Delta rbmA$ AI-2-responsive strain harboring
 282 chromosomal *Pbad-rbmA-3xFLAG*, treated as indicated. (E) Box plot showing the biofilm core
 283 cell density in the AI-2-responsive strain (denoted “Control”) and the $\Delta rbmA$ *Pbad-rbmA-3xFLAG*
 284 AI-2-responsive strain following the indicated treatments. Shown are the means \pm standard

285 deviations for $N = 3$ biological replicates. Unpaired *t*-tests were performed for statistical analyses.
286 In A-D, data points are colored by the kernel density estimate, which represents the probability
287 density function with respect to local biofilm density and distance to the biofilm core. **** $P \leq$
288 0.0001; *** $P \leq 0.001$; ** $P \leq 0.01$; * $P \leq 0.05$; ns $P > 0.05$. Norspermidine, Nspd; Arabinose, Ara;
289 Kernel density estimate, KDE.

290 Obvious candidates to connect norspermidine and quorum-sensing signaling to biofilm
291 densification are the biofilm matrix proteins Bap1 and RbmA, as expression of the genes encoding
292 them is activated in the high cell density and high norspermidine signaling regime (Fig. 2C).
293 Following treatment with both ligands, the $\Delta bap1$ strain exhibited no change in bulk biofilm
294 biomass or biofilm core density compared to the parent AI-2-responsive strain treated with both
295 ligands eliminating a role for Bap1 (Fig. S5A,B). By contrast, deletion of *rbmA* reduced peak
296 biofilm biomass in the high cell density and high norspermidine signaling regime (Fig. S5A).
297 Moreover, upon washing, biofilms formed by the $\Delta rbmA$ AI-2-responsive strain detached from the
298 substrate, likely because they are fragile due to decreased cell-cell adhesion (Fig. S5C) (29,30).
299 Synthetic induction of *rbmA* expression increased biofilm core density in a dose-dependent
300 manner (Fig. 4E), consistent with previous results (31). Thus, ligand-driven *rbmA* upregulation is
301 a potential mechanism that links the high norspermidine and high cell density quorum-sensing
302 signaling regime to changes in biofilm architecture. Indeed, when we matched RbmA-3xFLAG
303 levels in the norspermidine-treated $\Delta rbmA$ strain to the doubly ligand-treated parent strain using
304 a chromosomal *Pbad-rbmA-3xFLAG* construct (using 0.275% arabinose, Figure 4D), the spatial
305 density correlations and the biofilm core densities of the two strains became roughly equivalent
306 (Fig. 4C-E). Thus, increased *rbmA* expression largely explains the synergistic effects of
307 norspermidine and quorum-sensing signaling on biofilm biomass accumulation.

Discussion

308 In this study, we investigated the effects of simultaneously altering c-di-GMP and quorum-
309 sensing signaling on *V. cholerae* biofilm morphogenesis. Strikingly, we found that changing c-di-
310 GMP signaling through norspermidine supplementation had little effect on biofilm biomass in the
311 low cell density quorum-sensing signaling state but had a biofilm-promoting effect in the high cell
312 density quorum-sensing signaling state (Fig. 2). We demonstrated that the synergy between the
313 signaling pathways is a consequence of increased production of NspS and MbaA at high cell
314 density. Thus, under this condition, c-di-GMP levels can increase if norspermidine is present (Fig.
315 3). The effect of elevated c-di-GMP levels is activation of VpsR, which we infer undergoes positive
316 feedback and activates *rbmA* and *vps* operon gene expression both directly and indirectly via
317 induction of *vpsT* (Figs. 2, S4). Notably, our RNAseq results show that *vpsT* is most highly
318 expressed in the presence of norspermidine alone, yet biofilm biomass is highest following
319 norspermidine and AI-2 co-treatment. We infer that HapR-mediated repression is stronger than
320 VpsR-mediated activation of *vpsT*, even when high levels of c-di-GMP are present. Nonetheless,
321 when both ligands are present, the levels of VpsT and VpsR produced are sufficient to drive
322 increased biofilm biomass. The combined changes in gene expression in the high cell density
323 quorum-sensing and high norspermidine signaling state drive the formation of larger, denser
324 biofilms than those that form in the low cell density signaling state (Fig. 4). The major takeaway
325 from this research is that, remarkably, quorum sensing can either promote or suppress biofilm
326 biomass accumulation, depending on the presence or absence of environmental cues that
327 impinge on c-di-GMP signaling (Fig. 5).



328 **Fig. 5. Proposed model for the integration of quorum-sensing and c-di-GMP signaling in *V.*
 329 ***cholerae* biofilm morphogenesis.** At low cell density, HapR levels are low, and consequently,
 330 NspS-MbaA levels are low, biofilm genes are expressed, and biofilms form. As the bacterial
 331 population grows and cell density increases, HapR levels rise, and HapR activates *nspS* and
 332 *mbaA* expression. (Top) At high cell density, in the absence of norspermidine, the NspS-MbaA
 333 circuit is inactive, and HapR-mediated repression of biofilm gene expression causes dispersal.
 334 (Bottom) At high cell density, in the presence of norspermidine, the NspS-MbaA pathway is
 335 activated, and high levels of the Nspd-NspS-MbaA complex produce c-di-GMP that increases
 336 biofilm gene expression, leading to biofilm expansion and densification. Norspermidine, Nspd.**

337 Our findings imply that quorum sensing confers plasticity to the population-level decision
 338 to commit to the biofilm or the free-swimming state. In the absence of c-di-GMP-modulating
 339 signals, quorum sensing promotes the free-swimming state at high cell density, but via
 340 upregulation of c-di-GMP-metabolizing enzymes that detect environmental stimuli, quorum-

341 sensing signaling has the potential to drive the opposite output behavior of population-level
342 commitment to the biofilm state. It has long been known that quorum sensing controls the
343 expression of genes encoding over a dozen c-di-GMP-metabolizing enzymes (Fig. S6) (21).
344 However, the ramifications of this regulatory arrangement have remained mysterious prior to this
345 work. A previously reported model for c-di-GMP and quorum-sensing integration proposed that
346 quorum-sensing communication and detection of environmental stimuli like oxygen, polyamines,
347 nitric oxide, etc., independently contribute to alterations in c-di-GMP levels (32). Our results show
348 that, at least for the quorum-sensing and polyamine cues, this is not the case. Rather, the stimuli
349 act synergistically. Testing the generality of this model remains to be performed, however, the
350 possibility to do so is limited by the scarcity of known ligands that control diguanylate cyclase and
351 phosphodiesterase activities.

352 We wonder how the results presented here might extend to other bacteria. *V. cholerae* is
353 unusual in that individually, the high cell density quorum-sensing state and the high c-di-GMP
354 state promote opposite biofilm phenotypes. In other bacteria, such as *Pseudomonas aeruginosa*,
355 the high cell density quorum-sensing state and the high c-di-GMP state both independently
356 promote biofilm formation (33,34). In *P. aeruginosa*, the prevailing model for c-di-GMP signaling
357 and its influence on biofilm development is that c-di-GMP-metabolizing enzymes with specialized
358 sensory functions in biofilm formation (e.g., surface sensing) are upregulated and/or activated at
359 different points in the biofilm lifecycle, typically via two-component signal transduction pathways
360 (34). Thus, context-dependency is a known feature of c-di-GMP signaling in *P. aeruginosa* biofilm
361 morphogenesis, however, connections between quorum sensing and environmental stimuli that
362 promote changes in c-di-GMP levels and biofilm formation remain uncharacterized in *P.*
363 *aeruginosa*. Probing the interactions between quorum-sensing and c-di-GMP signaling in *P.*
364 *aeruginosa* and other species that occupy diverse niches and that have lifestyles that differ
365 dramatically from that of *V. cholerae* could deliver a unified picture of how the coordination of

366 sensory signaling systems is linked to the ecological and evolutionary roles that biofilms play
367 across the bacterial domain.

Methods

Bacterial strains, reagents, reporters, and western blotting procedures

368 The *V. cholerae* strain used in this study was O1 El Tor biotype C6706str2. Antibiotics
369 were used at the following concentrations: polymyxin B, 50 µg/mL; kanamycin, 50 µg/mL;
370 spectinomycin, 200 µg/mL; chloramphenicol, 1 µg/mL; and gentamicin, 5 µg/mL. Strains were
371 propagated at 30° C in liquid lysogeny broth (LB) with shaking or LB containing 1.5% agar for
372 plates. Strains used for reporter assays, imaging assays, and RNA isolation were grown in M9
373 minimal medium supplemented with 0.5% dextrose, 0.5% casamino acids, and 0.1 mM boric acid.
374 AI-2 (S-2-methyl-2,3,3,4-tetrahydroxytetrahydrofuran-borate) and the CqsS agonist 1-ethyl-N-[(4-
375 (propan-2-yl)phenyl]methyl]-1*H*-tetrazol-5-amine were synthesized as described previously (35–
376 38). Norspermidine (Millipore Sigma, I1006-100G-A), arabinose (Millipore Sigma, W325501), AI-
377 2, and the CqsS agonist were added at the concentrations designated in the figures or figure
378 legends at the initiation of the assay. c-di-GMP was measured as described previously (17,26).
379 Western blots for MbaA-3xFLAG, VpsT-3xFLAG, VpsR-3xFLAG, and RbmA-3xFLAG were
380 performed as described previously, using a monoclonal anti-FLAG-peroxidase antibody (Millipore
381 Sigma, #A8592; Danvers, MA, USA). RpoA served as the loading control and it was detected
382 using an anti-*Escherichia coli* RNA polymerase α primary antibody (Biolegend, #663104) and an
383 anti-mouse IgG HRP conjugate secondary antibody (Promega, #W4021) (13). For strains carrying
384 VpsT-3xFLAG, RbmA-3xFLAG, or VpsR-3xFLAG, prior to application of the anti-RpoA antibody,
385 the anti-FLAG-peroxidase antibody was stripped from the membranes by incubation at 25° C in
386 stripping buffer (15 g/L glycine, 1 g/L SDS, 10 mL/L Tween-20, diluted in water, buffered to pH =

387 2.2) for 15 min, followed by a second incubation with stripping buffer for 10 min, followed by two
388 10 min incubations in PBS, and finally two 5 min incubations in PBST.

DNA manipulation and strain construction

389 Modifications to the *V. cholerae* genome were generated by replacing genomic DNA with
390 linear DNA introduced by natural transformation as described previously (13,39,40). PCR and
391 Sanger sequencing (Genewiz) were used to verify genetic alterations. See S1 Table for primers
392 and g-blocks (IDT) and S2 Table for a list of strains used in this study. Constructs driven by the
393 *Pbad* promoter were introduced at the neutral locus *vc1807*. The *Pbad-nspS-mbaA* construct was
394 produced by replacing the native *nspS* promoter with *Pbad*.

Microscopy Analyses

395 Measurements of biofilm biomass were made as described previously (13) using bright
396 field microscopy with minimal modifications. In brief, single-plane images were acquired at 30 min
397 intervals on a Biotek Cytation 7 multimodal plate reader using an air immersion 20x objective lens
398 (Olympus, PL FL; NA: 0.45) with static incubation at 30° C. Analyses were performed using FIJI
399 software (Version 1.53c). Images in the time-series were smoothed using a Gaussian filter (σ =
400 10), followed by segmentation using an intensity threshold. The total amount of light attenuated
401 in each image after segmentation was summed to yield the biofilm biomass for the corresponding
402 time point.

403 For high resolution images of cells in biofilms (Figs. 4 and S5), samples were fixed by
404 treatment with 3.7% formaldehyde (Avantor, MFCD00003274) in PBS for 10 min. To terminate
405 fixation, samples were washed five times with PBS. Cells were subsequently stained with 1 μ g/mL
406 4',6-diamidino-2-phenylindole (DAPI) in PBS for 30 min at 25° C. Single-cell resolution images of
407 fixed samples were acquired using a DMI8 Leica SP-8 point scanning confocal microscope (Leica,
408 Wetzlar, Germany) equipped with a 63x water immersion objective (Leica, HC PL APO CS2; NA:
409 1.20). The excitation light source was a 405 nm diode laser and emitted light was detected by a
410 GaAsP spectral detector (Leica, HyD SP). Cell segmentation and biofilm parameter calculations

411 were performed using BiofilmQ (parameters Architecture_LocalDensity and Distance_ToBiofilm
412 CenterAtSubstrate) (31). All plots were generated using Python 3. Figures were assembled in
413 Inkscape (41,42).

RNA isolation and sequencing

414 Overnight cultures of the *V. cholerae* AI-2-responsive strain, grown in biological triplicate,
415 were diluted to $OD_{600} \sim 0.001$ in 5 mL of M9 medium. The subcultured cells were grown at 30° C
416 with shaking in the presence of the designated polyamine and/or AI-2 treatment to $OD_{600} = 0.1$.
417 Cells were harvested by centrifugation for 10 min at 4,000 RPM and resuspended in RNAProtect
418 (Qiagen). RNA was isolated using the RNeasy mini kit (Qiagen), remaining DNA was digested
419 using the TURBO DNA-free kit (Invitrogen), and the concentration and purity of RNA were
420 measured using a NanoDrop instrument (Thermo). Samples were flash frozen in liquid nitrogen
421 and stored at -80° C until they were shipped on dry ice to SeqCenter
422 (<https://www.seqcenter.com/rna-sequencing/>). The 12 million paired-end reads option and the
423 intermediate analysis package were selected for each sample. Quality control and adapter
424 trimming were performed with bcl2fastq (Illumina), while read mapping was performed with
425 HISAT2 (43). Read quantitation was performed using the Subread's featureCounts (44)
426 functionality, and subsequently, counts were loaded into R (R Core Team) and normalized using
427 the edgeR (45) Trimmed Mean of M values (TMM) algorithm. Values were converted to counts
428 per million (cpm), and differential expression analyses were performed using the edgeR Quasi-
429 Linear F-Test (qlfTest) functionality against treatment groups, as indicated. The results, presented
430 in Fig. 2C, were plotted using Python 3 (41).

Acknowledgements and Funding

431 The authors thank members of the Bassler group for insightful discussions. This work was
432 supported by the Howard Hughes Medical Institute, NSF grant MCB-2043238, NIH grant

433 2R37GM065859 (B.L.B.), and NIH grant 1K99AI158939 (A.A.B). The funders had no role in study
434 design, data collection and analysis, decision to publish, or preparation of the manuscript.

Literature Cited

1. Flemming HC, Wingender J, Szewzyk U, Steinberg P, Rice SA, Kjelleberg S. Biofilms: an emergent form of bacterial life. *Nat Rev Microbiol.* 2016 Sep;14(9):563–75.
2. Flemming HC, Wingender J. The biofilm matrix. *Nat Rev Microbiol.* 2010 Sep;8(9):623–33.
3. Mah TF, Pitts B, Pellock B, Walker GC, Stewart PS, O'Toole GA. A genetic basis for *Pseudomonas aeruginosa* biofilm antibiotic resistance. *Nature.* 2003 Nov 20;426(6964):306–10.
4. Shaw T, Winston M, Rupp CJ, Klapper I, Stoodley P. Commonality of elastic relaxation times in biofilms. *Phys Rev Lett.* 2004 Aug 27;93(9):098102.
5. Costerton JW, Stewart PS, Greenberg EP. Bacterial Biofilms: A Common Cause of Persistent Infections. *Science.* 1999 May 21;284(5418):1318–22.
6. Mukherjee S, Bassler BL. Bacterial quorum sensing in complex and dynamically changing environments. *Nat Rev Microbiol.* 2019;17(6):371–82.
7. Miller MB, Bassler BL. Quorum Sensing in Bacteria. *Annu Rev Microbiol.* 2001;55(1):165–99.
8. Herzog R, Peschek N, Fröhlich KS, Schumacher K, Papenfort K. Three autoinducer molecules act in concert to control virulence gene expression in *Vibrio cholerae*. *Nucleic Acids Res.* 2019 Apr 8;47(6):3171–83.
9. Freeman JA, Bassler BL. Sequence and function of LuxU: a two-component phosphorelay protein that regulates quorum sensing in *Vibrio harveyi*. *J Bacteriol.* 1999 Feb;181(3):899–906.

10. Freeman JA, Bassler BL. A genetic analysis of the function of LuxO, a two-component response regulator involved in quorum sensing in *Vibrio harveyi*. *Mol Microbiol*. 1999 Jan;31(2):665–77.
11. Lenz DH, Mok KC, Lilley BN, Kulkarni RV, Wingreen NS, Bassler BL. The small RNA chaperone Hfq and multiple small RNAs control quorum sensing in *Vibrio harveyi* and *Vibrio cholerae*. *Cell*. 2004 Jul 9;118(1):69–82.
12. Papenfort K, Bassler BL. Quorum sensing signal-response systems in Gram-negative bacteria. *Nat Rev Microbiol*. 2016 Aug 11;14(9):576–88.
13. Bridges AA, Bassler BL. The intragenus and interspecies quorum-sensing autoinducers exert distinct control over *Vibrio cholerae* biofilm formation and dispersal. *PLoS Biol*. 2019;17(11):e3000429.
14. Bernier SP, Ha DG, Khan W, Merritt JH, O'Toole GA. Modulation of *Pseudomonas aeruginosa* surface-associated group behaviors by individual amino acids through c-di-GMP signaling. *Res Microbiol*. 2011 Sep;162(7):680–8.
15. Carlson HK, Vance RE, Marletta MA. H-NOX regulation of c-di-GMP metabolism and biofilm formation in *Legionella pneumophila*. *Mol Microbiol*. 2010;77(4):930–42.
16. Kanazawa T, Ren S, Maekawa M, Hasegawa K, Arisaka F, Hyodo M, et al. Biochemical and Physiological Characterization of a BLUF Protein–EAL Protein Complex Involved in Blue Light-Dependent Degradation of Cyclic Diguanylate in the Purple Bacterium *Rhodopseudomonas palustris*. *Biochemistry*. 2010 Dec 21;49(50):10647–55.

17. Bridges AA, Prentice JA, Fei C, Wingreen NS, Bassler BL. Quantitative input–output dynamics of a c-di-GMP signal transduction cascade in *Vibrio cholerae*. *PLOS Biol*. 2022 Mar 18;20(3):e3001585.
18. Tuckerman JR, Gonzalez G, Sousa EHS, Wan X, Saito JA, Alam M, et al. An Oxygen-Sensing Diguanylate Cyclase and Phosphodiesterase Couple for c-di-GMP Control. *Biochemistry*. 2009 Oct 20;48(41):9764–74.
19. Ha DG, O'Toole GA. c-di-GMP and its Effects on Biofilm Formation and Dispersion: a *Pseudomonas Aeruginosa* Review. *Microbiol Spectr*. 2015 Apr;3(2):MB-0003-2014.
20. Jenal U, Reinders A, Lori C. Cyclic di-GMP: second messenger extraordinaire. *Nat Rev Microbiol*. 2017 May;15(5):271–84.
21. Waters CM, Lu W, Rabinowitz JD, Bassler BL. Quorum Sensing Controls Biofilm Formation in *Vibrio cholerae* through Modulation of Cyclic Di-GMP Levels and Repression of *vpsT*. *J Bacteriol*. 2008 Apr 1;190(7):2527–36.
22. Srivastava D, Harris RC, Waters CM. Integration of cyclic di-GMP and quorum sensing in the control of *vpsT* and *aphA* in *Vibrio cholerae*. *J Bacteriol*. 2011 Nov;193(22):6331–41.
23. Hammer BK, Bassler BL. Quorum sensing controls biofilm formation in *Vibrio cholerae*. *Mol Microbiol*. 2003;50(1):101–4.
24. Beyhan S, Bilecen K, Salama SR, Casper-Lindley C, Yildiz FH. Regulation of Rugosity and Biofilm Formation in *Vibrio cholerae*: Comparison of *VpsT* and *VpsR* Regulons and Epistasis Analysis of *vpsT*, *vpsR*, and *hapR*. *J Bacteriol*. 2007 Jan 15;189(2):388–402.

25. Zhou H, Zheng C, Su J, Chen B, Fu Y, Xie Y, et al. Characterization of a natural triple-tandem c-di-GMP riboswitch and application of the riboswitch-based dual-fluorescence reporter. *Sci Rep.* 2016 Feb 19;6(1):20871.

26. Bridges AA, Bassler BL. Inverse regulation of *Vibrio cholerae* biofilm dispersal by polyamine signals. Laub MT, Storz G, Michael A, Mandel M, editors. *eLife.* 2021 Apr 15;10:e65487.

27. Karatan E, Duncan TR, Watnick PI. NspS, a Predicted Polyamine Sensor, Mediates Activation of *Vibrio cholerae* Biofilm Formation by Norspermidine. *J Bacteriol.* 2005 Nov;187(21):7434–43.

28. Casper-Lindley C, Yildiz FH. VpsT Is a Transcriptional Regulator Required for Expression of vps Biosynthesis Genes and the Development of Rugose Colonial Morphology in *Vibrio cholerae* O1 El Tor. *J Bacteriol.* 2004 Mar;186(5):1574–8.

29. Yan J, Sharo AG, Stone HA, Wingreen NS, Bassler BL. *Vibrio cholerae* biofilm growth program and architecture revealed by single-cell live imaging. *Proc Natl Acad Sci.* 2016 Sep 6;113(36):E5337–43.

30. Hartmann R, Singh PK, Pearce P, Mok R, Song B, Díaz-Pascual F, et al. Emergence of three-dimensional order and structure in growing biofilms. *Nat Phys.* 2019 Apr 26;15(3):251–6.

31. Hartmann R, Jeckel H, Jelli E, Singh PK, Vaidya S, Bayer M, et al. Quantitative image analysis of microbial communities with BiofilmQ. *Nat Microbiol.* 2021 Feb;6(2):151–6.

32. Srivastava D, Waters CM. A Tangled Web: Regulatory Connections between Quorum Sensing and Cyclic Di-GMP. *J Bacteriol.* 2012 Sep;194(17):4485–93.

33. De Kievit TR. Quorum sensing in *Pseudomonas aeruginosa* biofilms. *Environ Microbiol*. 2009;11(2):279–88.
34. Valentini M, Filloux A. Biofilms and Cyclic di-GMP (c-di-GMP) Signaling: Lessons from *Pseudomonas aeruginosa* and Other Bacteria. *J Biol Chem*. 2016 Jun 10;291(24):12547–55.
35. Higgins DA, Pomianek ME, Kraml CM, Taylor RK, Semmelhack MF, Bassler BL. The major *Vibrio cholerae* autoinducer and its role in virulence factor production. *Nature*. 2007 Dec 6;450(7171):883–6.
36. Semmelhack MF, Campagna SR, Federle MJ, Bassler BL. An Expeditious Synthesis of DPD and Boron Binding Studies. *Org Lett*. 2005 Feb 1;7(4):569–72.
37. Ng WL, Wei Y, Perez LJ, Cong J, Long T, Koch M, et al. Probing bacterial transmembrane histidine kinase receptor–ligand interactions with natural and synthetic molecules. *Proc Natl Acad Sci*. 2010 Mar 23;107(12):5575–80.
38. Hurley A, Bassler BL. Asymmetric regulation of quorum-sensing receptors drives autoinducer-specific gene expression programs in *Vibrio cholerae*. *PLOS Genet*. 2017 May 26;13(5):e1006826.
39. Dalia AB. Natural Cotransformation and Multiplex Genome Editing by Natural Transformation (MuGENT) of *Vibrio cholerae*. In: Sikora AE, editor. *Vibrio Cholerae: Methods and Protocols* [Internet]. New York, NY: Springer; 2018 [cited 2022 Jun 21]. p. 53–64. (Methods in Molecular Biology). Available from: https://doi.org/10.1007/978-1-4939-8685-9_6

40. Dalia AB, McDonough E, Camilli A. Multiplex genome editing by natural transformation. *Proc Natl Acad Sci U S A*. 2014 Jun 17;111(24):8937–42.
41. The Python Language Reference — Python 3.10.5 documentation [Internet]. [cited 2022 Jun 21]. Available from: <https://docs.python.org/3/reference/>
42. Developers IW. Draw Freely | Inkscape [Internet]. [cited 2022 Jun 21]. Available from: <https://inkscape.org/>
43. Kim D, Paggi JM, Park C, Bennett C, Salzberg SL. Graph-based genome alignment and genotyping with HISAT2 and HISAT-genotype. *Nat Biotechnol*. 2019 Aug;37(8):907–15.
44. Liao Y, Smyth GK, Shi W. featureCounts: an efficient general purpose program for assigning sequence reads to genomic features. *Bioinformatics*. 2014 Apr 1;30(7):923–30.
45. Robinson MD, McCarthy DJ, Smyth GK. edgeR: a Bioconductor package for differential expression analysis of digital gene expression data. *Bioinformatics*. 2010 Jan 1;26(1):139–40.